Materials International
Open Access Journal (ISSN: 2668-5728)

Article
Volume 7, Issue 2, 2025, 13
https://doi.org/10.33263/Materials72.013

Do Transition Metals (Cobalt, Copper, Zinc) Dope on BN-Nanosensor Enhance Nitric Oxide Detection? A Promising Technique for Designing Sustainable Nanodetector

Fatemeh Mollaamin [1,*]

[1] Department of Biomedical Engineering, Faculty of Engineering and Architecture, Kastamonu University, Kastamonu, Turkey
* Correspondence: fmollaamin@kastamonu.edu.tr/smollaamin@gmail.com;

Scopus Author ID 35848813100
Received: 19.10.2024; Accepted: 2.01.2025; Published: 13.02.2025

Abstract: Toxic gas of nitric oxide (NO) adsorbed on the transition metals (Co, Cu, Zn)-doped boron nitride nanocage (B_5N_{10}_NC) has been investigated using density functional theory (DFT). The results denote that NO@X–B_4N_{10}_NC complexes are stable through the adsorption site in the center of the cage ring. The partial density of states (PDOS) can evaluate a determined charge assembly between gas molecules and X–B_4N_{10}_NC, which indicates the competition among dominant complexes. Based on NQR analysis, X-doped on B_5N_{10}_NC has shown the lowest electric potential and atomic charge fluctuation. Furthermore, the reported results of NMR spectroscopy have exhibited that the yield of electron-accepting for doping atoms on the X–B_4N_{10}_NC through the adsorption process can be ordered as: Co > Cu >Zn that exhibits the strength of covalent bond between cobalt, copper, zinc and NO. The adsorption of NO can introduce spin polarization on the X–B_4N_{10}_NC, which specifies that these surfaces may be employed as magnetic scavenging surfaces as a gas detector. Regarding IR spectroscopy, doped nanocages of Co–B_4N_{10}_NC, Cu–B_4N_{10}_NC, and Zn–B_4N_{10}_NC, respectively, have the most fluctuations and the highest adsorption tendency for gas molecules, which can address specific questions on the individual effect of charge carriers (gas molecule-nanocage), as well as doping atoms on the overall structure. Based on the results of $\Delta G^{o}_{ads.}$ Amounts in this research, the maximum efficiency of Co, Cu, and Zn atoms doping of B_5N_{10}_NC for gas molecules adsorption depends on the covalent bond between NO molecules and X–B_4N_{10}_NC as a potent sensor for air pollution removal. Finally, the high selectivity of atom-doped on boron nitride nanocage (gas sensor) for gas molecule adsorption has resulted in Cu>>Co>Zn.

Keywords: environmental pollution; gas detecting; nanomaterials; transition metals; DFT.

1. Introduction

Boron nitride nanomaterials have been used owing to their unparalleled specifications of eco-friendly attributes for pollutant adsorption and semiconducting properties [1–4].

Boron nitride nanomaterials usually exhibit semi-leading behavior, which is considered a proper alternative to carbon nanotubes. The properties of boron and nitrogen atoms, which are the first neighbors of carbon in the periodic table, make boron nitride an interesting subject of numerous studies [5–7]. In recent years, different investigations on the adsorption of chemical contaminants and applying various boron nitride nanostructures as adsorbents for water purification have been studied [8–10].

Various physical shapes of boron nitride (BN)-based nano adsorbents such as nanoparticles, fullerenes, nanotubes, nanofibers, nanoribbons, nanosheets, nanomeshes, nanoflowers, and hollow spheres have been broadly considered possible adsorbents owing to their exceptional characteristics such as large surface area, structural variability, great chemical/mechanical strength, abundant structural defects, high reactive sites, and functional groups [11,12].

Particularly, this research work aims to assess the influences of doping atoms of Co, Cu, and Zn on the B_5N_{10}_NC for increasing gas detection through measurement of some parameters containing charge transfer, electric potential, electromagnetic and thermodynamic properties, surface area, functional group and examine the removal of selected toxic gas of NO during the adsorption process.

2. Materials and Methods

2.1. NO adsorption on X–B4N10_NC.

The aim of this study is to remove NO from the air through an eco-friendly approach by using (Co, Cu, Zn)-doped B_5N_{10}_NC (Figure 1).

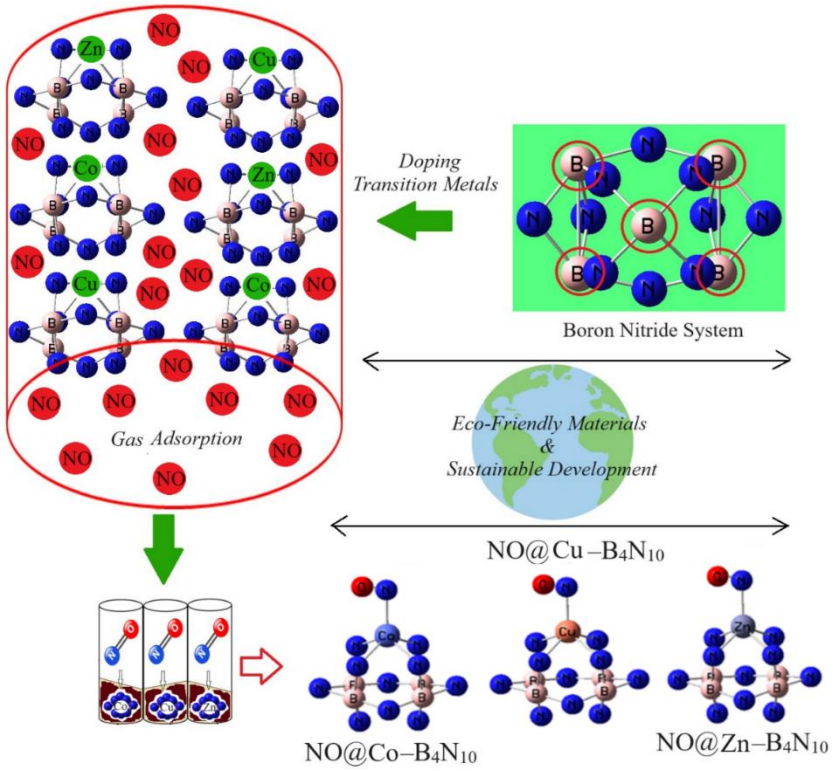

Figure 1. Application of X–B_4N_{10}_NC towards NO adsorption and formation of: NO@Co–B_4N_{10}_NC, NO@Cu–B_4N_{10}_NC, NO@Zn–B_4N_{10}_NC complexes using CAM–B3LYP–D3/6–311+G (d,p), LANL2DZ calculation. (Note: the sign of adsorption is @).

Boron nitride nanocage was modeled in the presence of cobalt, copper, and zinc doping atoms, which can augment the gas-sensing potential of BN-nanocage. In our research, sample characterization was performed using CAM–B3LYP–D3 /EPR–3, LANL2DZ level of theory.

Figure 1 has shown the process of NO adsorption on the X–B_4N_{10}_NC surface, which describes the formation of NO@Co–B_4N_{10}_NC, NO@Cu–B_4N_{10}_NC, NO@Zn–B_4N_{10}_NC by molecular modeling computations.

The charge distribution of the mentioned complexes is calculated using the Bader charge analysis [13].

The trapping of NO molecules by X– B_4N_{10}_NC (X= Co, Cu, Zn) was successfully incorporated due to binding formation consisting of N→ Co, N→ Cu, N→ Zn (Figure 1).

2.2. Application of density functional theory approach.

Hohenberg-Kohn (HK) functions have rigidly made the electronic density permissible as a fundamental variable to electronic and structure computations. In other words, the development of the applied density functional theory (DFT) methodology only became notable after W. Kohn and L. J. Sham released their reputable series of equations, which are introduced as Kohn-Sham (KS) equations [14–19].

Considering the electronic density within the KS image, we are able to see a remarkable reduction in quantum computing. Thus, the KS methodology lightens the route for pursuing systems that cannot be discussed by conventional ab initio methodologies. "Kohn and Sham" introduces the solution, which brings up the mono-electronic orbitals to account for the kinetic energy in a simple and relatively exact way by finding a residual modification that might be computed apart. So, one starts with a reference model of M with non-interacting electrons related to the external potential v_s and with Hamiltonian [18,19]:

$$\hat{H}_s = -\sum_i^M \frac{1}{2}\overline{\nabla}_i^2 + \sum_i^M v_s(\vec{r}_i) = \sum_i^M \hat{h}_s ; \quad \hat{h}_s = -\frac{1}{2}\overline{\nabla}_i^2 + v_s(\vec{r}_i) \qquad (1)$$

By representing the single-particle orbitals ψ_i, all electronic densities physically acceptable for the system of "non-interacting" electrons are written in the equation (2):

$$\rho(\vec{r}) = \sum_i^M |\psi_i(\vec{r})|^2 \qquad (2)$$

Finally, the total energy could be measured by the KS method due to the equation (3):

$$E[\rho] = \sum_i^M n_i \langle \psi_i \left| -\frac{1}{2}\overline{\nabla}^2 + v_{ext}(\vec{r}) + \frac{1}{2}\int \frac{\rho(\vec{r}')}{|\vec{r}-\vec{r}'|}\, d\vec{r}' \right| \psi_i \rangle + E_{xc}[\rho] + \frac{1}{2}\sum_\beta^N \sum_{\alpha\neq\beta}^N \frac{Z_\alpha Z_\beta}{|\vec{R}_\alpha - \vec{R}_\beta|} \qquad (3)$$

Therefore, the precise exchange energy function is described by the Kohn–Sham orbitals instead of the density, which is cited as the indirect density functional. This research has employed the penetration of the hybrid functional of a three-parameter basis set of "B3LYP (Becke, three-parameter, Lee, Yang, Parr)" within the conception of DFT upon theoretical computations [20,21]. The popular B3LYP and exchange-correlation functional become based on equation (4) [22–24]:

$$E_{XC}^{B3LYP} = (1-\alpha)E_x^{LSDA} + \alpha E_x^{HF} + b\Delta E_x^B + (1-c)E_c^{LSDA} + cE_c^{LYP} \qquad (4)$$

$\alpha = 0.20, b = 0.72, c = 0.81$ shows a generalized gradient approximation: the Becke ex-change functional [25] and the correlation functional of Lee, Yang, and Parr [26] for B3LYP and E_c^{LSDA} is the VWN local spin density approximation to the correlation functional [27].

In this article, the rigid PES using DFT calculations was computed using Gaussian 16 revision C.01 software [28]. The input Z-matrix for adsorption of NO molecules by the X–B_4N_{10}_NC has been designed with GaussView 6.1 [29] using 6–311+G (d,p), EPR–3, and LANL2DZ basis sets. In this study, the interaction between gas molecules and X–B_4N_{10}_NC was modeled and analyzed. As was revealed by DFT-based analysis, the potency of X–B_4N_{10}_NC for grabbing NO molecules was determined mainly by the electronegativity of the functional groups, as well as the interaction between the X–B_4N_{10}_NC and the NO molecules.

3. Results and Discussion

One of the most dominant gas pollutants in the air is nitric oxide. The data has evaluated the efficiency of boron nitride nanocages doped with Co, Cu, and Zn for gas detection. The chemisorptive nature of the bond among the gas molecules with boron and nitrogen elements can be remarked on through the equilibrium distribution of doping atoms, B_5N_{10}_NC, and a monolayer attribute.

3.1. PDOS and electronic evaluating.

The electronic structures of NO adsorption by X (X= Co, Cu, Zn)-doped B_5N_{10}_NC as the selective sensor for detecting and grabbing gas molecules in the air have been characterized using CAM–B3LYP–D3/6–311+G (d,p), LANL2DZ level of theory.

Figure 2 (a–f) shows the projected density of state (PDOS) of NO@ X – B_4N_{10}_NC through gas molecules adsorption. The appearance of the energy states (*p*-orbital) of N, O and (*d*-orbital) of Co, Cu, Zn within the gap of X – B_4N_{10}_NC induces the system's reactivity. It is clear from the Figure that after trapping with gas molecules, d-orbital contributes significantly to the unoccupied level. Therefore, the curve of partial PDOS has described that the *p* states of N atoms in gas molecules and *d*-orbital in Co, Cu, Zn transition metals in X–B_4N_{10}_NC overcome due to the conduction band (Figure 2a–c). A distinguished adsorption trait might be seen in NO@X–B_4N_{10}_NC because of the potent interaction between the *p* states of the nitrogen atom and the *d* states of Co, Cu, and Zn in X–B_4N_{10}_NC complexes.

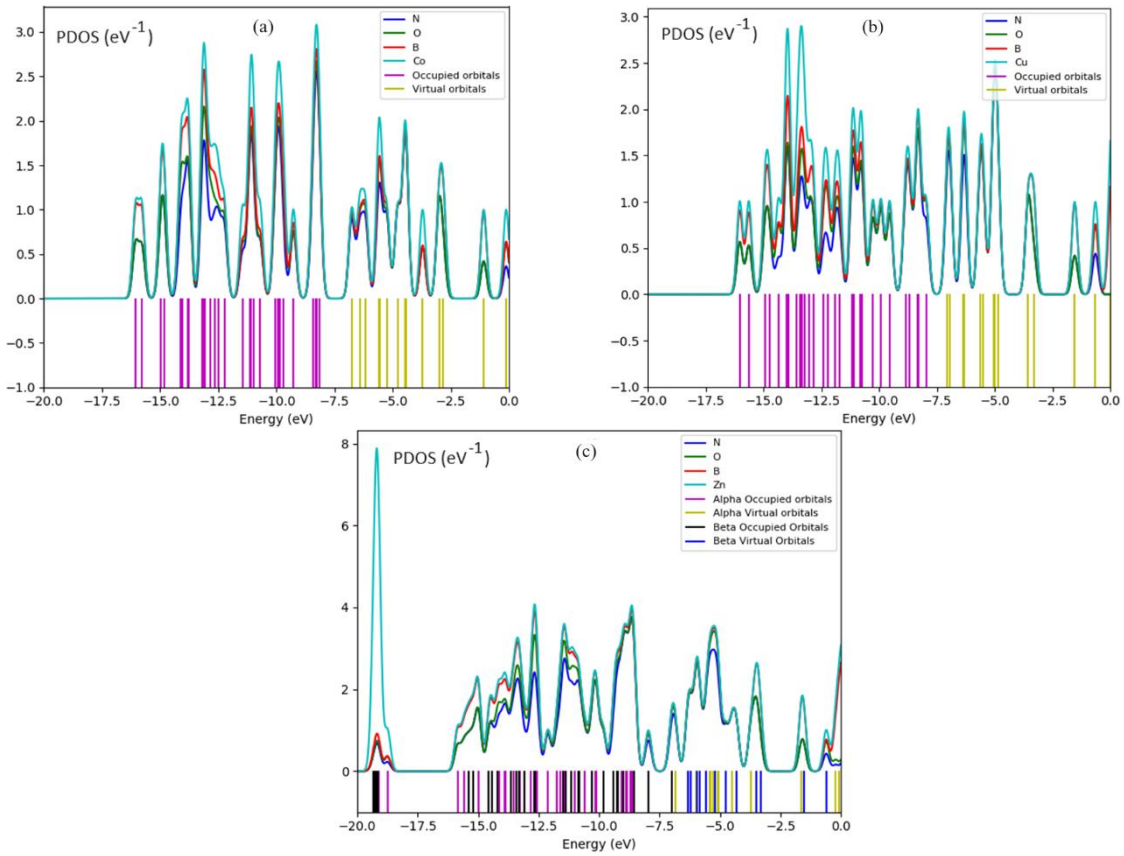

Figure 2. PDOS graph of NO adsorbed on X–B_4N_{10}_NC including **(a)** NO@ Co–B_4N_{10}_NC; **(b)** NO@ Cu–B_4N_{10}_NC; **(c)** NO@ Zn–B_4N_{10}_NC complexes by CAM–B3LYP–D3/6–311+G (d,p), LANL2DZ.

Figures 2(a–c) show that NO@ Co–B_4N_{10}_NC, NO@Cu–B_4N_{10}_NC, and NO@Zn–B_4N_{10}_NC complexes through the gas molecule adsorption, respectively, have the most

contribution at the middle of the conduction band between –5 to –15 eV, while contribution of boron and nitrogen states are enlarged and similar together, and the interfacial electronic of B_4N_{10}_NC depicts a criterion for NO adsorption. NO@ Co–B_4N_{10}_NC (Figure 2a) has exhibited four strong peaks around –8, –10, –11.5, and –14.5 eV through the graphs for the Co atom. Furthermore, the Cu graph with two sharp peaks around –14 and –14.5 eV in NO@ Cu–B_4N_{10}_NC (Figure 2b) has been shown. However, the Zn graph in NO@ Zn–B_4N_{10}_NC (Figure 2c) with one sharp peak around –19.5 eV attracts our attention. Therefore, the order potency of gas adsorption by doping atoms of Co, Cu, Zn on X–B_4N_{10}_NC based on the PDOS might be shifted as: Cu–B_4N_{10}_NC>>Co–B_4N_{10}_NC> Zn–B_4N_{10}_NC.

3.2. Insight to nuclear quadrupole resonance.

As the electric field gradient (EFG) at the citation of the nucleus in NO is allocated by the valence electrons twisted in the attachment with close nuclei of X–B_4N_{10}_NC through trapping of gas molecules, the nuclear quadrupole resonance (NQR) frequency at which transitions occur is particular for NO@X–B_4N_{10}_NC complexes (Table1). The NQR method is related to the multipole expansion in Cartesian coordinates as the equation (5) [30,31]:

$$V(r) = V(0) + \left[\left(\frac{\partial V}{\partial x_i}\right)\Big|_0 . x_i\right] + \frac{1}{2}\left[\left(\frac{\partial^2 V}{\partial x_i x_j}\right)\Big|_0 . x_i x_j\right] + \cdots (5)$$

Regarding a simplification of the equation (5), there are only the second derivatives related to the identical variable for the potential energy [30,31]:

$$U = -\frac{1}{2}\int_{\mathcal{D}} d^3\, r\, \rho_r \left[\left(\frac{\partial^2 V}{\partial x_i^2}\right)\Big|_0 . x_i^2\right] = -\frac{1}{2}\int_{\mathcal{D}} d^3\, r\, \rho_r \left[\left(\frac{\partial E_i}{\partial x_i}\right)\Big|_0 . x_i^2\right] =$$
$$-\frac{1}{2}\left(\frac{\partial E_i}{\partial x_i}\right)\Big|_0 . \int_{\mathcal{D}} d^3\, r\, [\rho(r) . x_i^2] \quad (6)$$

There are two parameters that must be obtained from NQR experiments: the quadrupole coupling constant, χ, and the asymmetry parameter of the EFG tensor η:

$$\chi = {e^2 Q q_{zz}}/{h} \quad (7)$$
$$\eta = {q_{xx} - q_{yy}}/{q_{zz}} \quad (8)$$

where q_{ii} (q_{xx}, q_{yy}, q_{zz}) are ingredients of the EFG tensor at the quadrupole nucleus determined in the EFG principal axes system, Q is the nuclear quadrupole moment, e is the proton charge, and h is the Planck's constant [32,33].

In this research article, the electric potential as the quantity of work energy through carrying over the electric charge from one position to another position in the essence of the electric field has been evaluated for NO@Co–B_4N_{10}_NC, NO@Cu–B_4N_{10}_NC, and NO@ Zn–B_4N_{10}_NC complexes (Table1).

Table1. The electric potential (a.u.) and Bader charge (e) through NQR for NO@Co–B_4N_{10}_NC, NO@Cu–B_4N_{10}_NC, and NO@Zn–B_4N_{10}_NC complexes using CAM–B3LYP–D3/EPR–3, LANL2DZ methods.

Co–B_4N_{10}_NC			**Cu–B_4N_{10}_NC**			**Zn–B_4N_{10}_NC**		
Atom	**Q**	**E_p**	**Atom**	**Q**	**E_p**	**Atom**	**Q**	**E_p**
N1	0.0813	-18.1696	N1	0.0377	-18.1784	N1	-0.0503	-18.2247
O2	-0.1111	-22.1930	O2	-0.0847	-22.1827	O2	-0.0987	-22.1976
B3	0.1511	-11.2799	B3	0.1439	-11.2831	B3	0.1150	-11.2782
N4	-0.0547	-18.2763	N4	-0.0320	-18.2747	N4	-0.0185	-18.2727
N5	-0.0626	-18.2520	N5	-0.0657	-18.2511	N5	-0.0436	-18.2528
B6	0.1449	-11.2800	B6	0.1362	-11.2829	B6	0.1141	-11.2787
B7	0.1460	-11.2798	B7	0.1301	-11.2822	B7	0.1127	-11.2786
B8	0.1462	-11.2809	B8	0.1247	-11.2809	B8	0.1128	-11.2786

Co–B_4N_{10}_NC			Cu–B_4N_{10}_NC			Zn–B_4N_{10}_NC		
Atom	**Q**	**E_p**	**Atom**	**Q**	**E_p**	**Atom**	**Q**	**E_p**
N9	-0.0739	-18.2786	N9	-0.0631	-18.273	N9	-0.0645	-18.2693
N10	-0.0678	-18.2558	N10	-0.0536	-18.2432	N10	-0.0414	-18.25
N11	-0.1124	-18.2576	N11	-0.1440	-18.2666	N11	-0.2080	-18.2814
N12	-0.125	-18.2642	N12	-0.1344	-18.2611	N12	-0.2116	-18.2823
N13	-0.1081	-18.257	N13	-0.1352	-18.2648	N13	-0.2026	-18.2819
N14	-0.1174	-18.2619	N14	-0.1410	-18.2634	N14	-0.2102	-18.2826
Co15	0.2962	-21.0329	Cu15	0.3710	-26.0693	Zn15	0.7768	-16.175
N16	-0.0817	-18.2785	N16	-0.0604	-18.273	N16	-0.0642	-18.2689
N17	-0.0510	-18.2718	N17	-0.0294	-18.2757	N17	-0.0174	-18.2724
N1	0.0813	-18.1696	N1	0.0377	-18.1784	N1	-0.0503	-18.2247

Table 1 investigates the Bader charge and electronic potential properties of Co, Cu, Zn, and B, N in X– B4N10_NC and N, O of NO molecules trapped on doped-boron nitride nanocages. The amounts indicate that with increasing the negative charge of different atoms, the electric potential resulting from NQR calculations increases. Moreover, the doping atoms of Co(15), Cu(15), and Zn(15) on the B_5N_{10}_NC have shown the most potential for accepting the electron from electron donors of N(1) and O (2) during NO adsorption on the X–B_4N_{10}_NC surfaces (Table 1).

Furthermore, in Figures 3 (a–c), it has been sketched the electric potential of NQR for some atoms of Co, Cu, Zn/B, N in X– B_4N_{10}_NC and N, O of NO trapped on doped-boron nitride nanocages which have been calculated by CAM–B3LYP–D3/EPR–3, LANL2DZ methods.

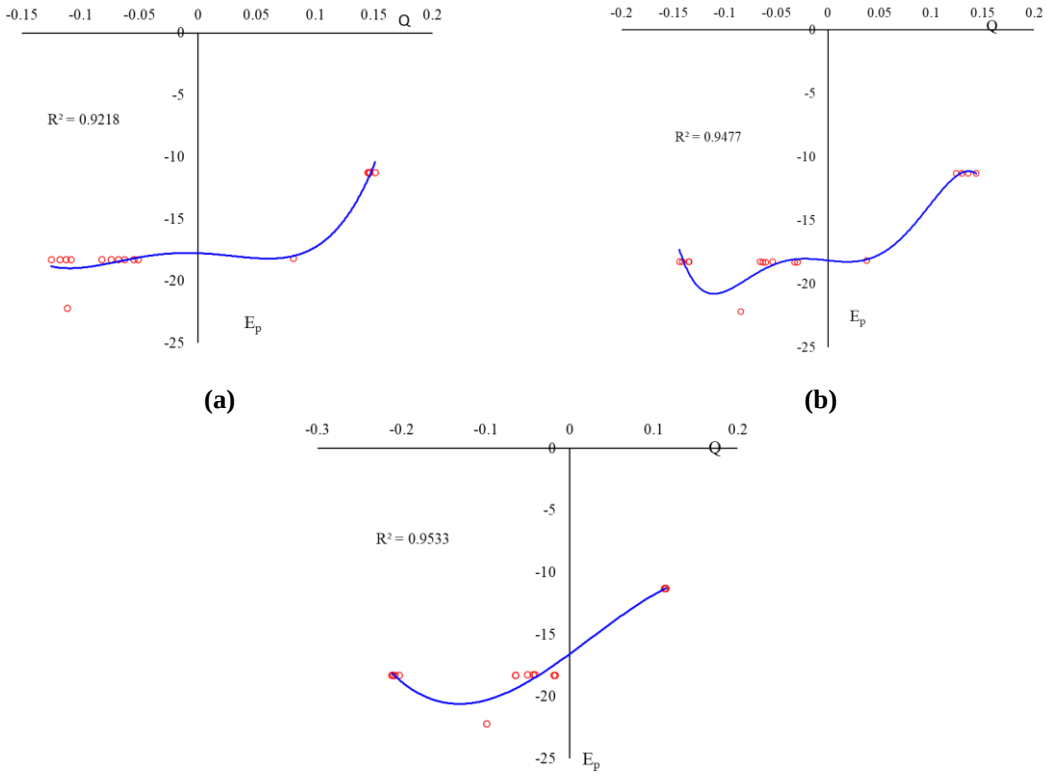

Figure 3. Electric potential (a.u.) versus Bader charge (coulomb) through NQR calculation for **(a)** NO@ Co–B_4N_{10}_NC; **(b)** NO@ Cu–B_4N_{10}_NC; **(c)** NO@ Zn–B_4N_{10}_NC complexes by CAM–B3LYP–D3/EPR–3, LANL2DZ.

NO adsorption on the Co–B_4N_{10}_NC in Figure 3a has illustrated the highest sensing of R^2 = 0.9218. In addition, Figures 3b and c have shown that NO@ Cu–B_4N_{10}_NC and NO @

Zn–B_4N_{10}_NC, respectively, have a good detection of NO removal from polluted air through the relation coefficients of $R^2 = 0.9477$ and $R^2 = 0.9533$.

It's vivid that the curve of X–B_4N_{10}_NC is waved by NO molecules. The fluctuated peaks for the electric potential have been shown around NO trapping on the X–B_4N_{10}_NC, which demonstrates the electron-accepting specifications of nitrogen and oxygen versus the cobalt, copper, and zinc doped on the B_4N_{10}_NC (Figure 3a–c). Besides, it can be considered that transition metals as ferromagnetic semiconductors in the functionalized B_4N_{10}_NC might have more impressive sensitivity for accepting the electrons from NO by Co, Cu, and Zn in the process of adsorption mechanism.

Table 1 has shown that cobalt-doped on B_5N_{10}_NC has the lowest fluctuation between Bader charge versus the electric potential extracted from NQR parameters and the highest negative atomic charge of 0.2962 coulomb in NO@Co–B_4N_{10}_NC can be an appropriate option with the highest tendency for electron accepting in the adsorption current (Table 1). In addition, the adsorbents of copper with 0.3710 coulomb and zinc with 0.7768 coulomb, respectively, have the most tendency to be electron acceptors. The uptake of gas molecules has been known to be associated with X–B_4N_{10}_NC, indicating that the adsorbed NO molecules on the X–doped nanocage can be internalized through a different pathway from pristine nanocage.

3.3. Analysis of nuclear magnetic resonance spectra.

Based on resulted amounts, nuclear magnetic resonance (NMR) spectra of X–B_4N_{10}_NC (X= Co, Cu, Zn) as the potent sensor for adsorbing NO can unravel the efficiency of X–B_4N_{10}_NC for detecting and removing this hazardous gas from polluted air as an eco-friendly approach.

From the DFT calculations, it has been attained the chemical shielding (CS) tensors in the principal axes system to estimate the isotropic chemical shielding (CSI) and the anisotropic chemical shielding (CSA) [34]:

$$\sigma_{iso} = (\sigma_{11} + \sigma_{22} + \sigma_{33})/3 \quad (9)$$

$$\sigma_{aniso} = \sigma_{33} - (\sigma_{22} + \sigma_{11})/2 \quad (10)$$

The NMR data of isotropic (σ_{iso}) and anisotropic shielding tensors (σ_{aniso}) for gas molecules trapped in the X–B_4N_{10}_NC towards formation of NO@Co–B_4N_{10}_NC, NO@Cu–B_4N_{10}_NC, and NO@Zn–B_4N_{10}_NC complexes has been computed by Gaussian 16 revision C.01 program package [28] and been shown in Table 2.

Table 2. NMR data of shielding tensors for selected atoms of NO@Co–B_4N_{10}_NC, NO@Cu–B_4N_{10}_NC, and NO@Zn–B_4N_{10}_NC complexes using CAM–B3LYP–D3/6–311+G (d,p), LANL2DZ calculation.

Co–B_4N_{10}_NC			**Cu–B_4N_{10}_NC**			**Zn–B_4N_{10}_NC**		
Atom	**σ_{iso}**	**σ_{aniso}**	**Atom**	**σ_{iso}**	**σ_{aniso}**	**Atom**	**σ_{iso}**	**σ_{aniso}**
N1	6235.13	21991.86	N1	63293.00	94223.48	N1	1551.16	1716.94
O2	13191.61	46595.00	O2	88823.60	132087.84	O2	1866.55	1659.43
B3	315.80	857.56	B3	31.0022	237.228	B3	59.21	86.06
N4	11531.79	25317.62	N4	3081.29	26445.87	N4	867.69	1132.70
N5	18262.38	59345.21	N5	2474.98	20423.95	N5	80.45	310.76
B6	371.00	784.1426	B6	39.79	210.98	B6	59.63	89.72
B7	322.72	820.1116	B7	66.86	321.73	B7	58.66	84.79
B8	351.29	762.9027	B8	1.84	182.22	B8	58.32	90.12
N9	2775.17	43699.70	N9	1189.16	18670.09	N9	270.49	738.94
N10	16350.09	52405.72	N10	2089.78	23940.52	N10	113.63	385.12
N11	2593.17	5918.10	N11	1208.41	5659.78	N11	913.16	606.23
N12	3290.23	6195.62	N12	4479.93	27757.65	N12	967.93	781.41

Co–B_4N_{10}_NC			Cu–B_4N_{10}_NC			Zn–B_4N_{10}_NC		
Atom	**σ_{iso}**	**σ_{aniso}**	**Atom**	**σ_{iso}**	**σ_{aniso}**	**Atom**	**σ_{iso}**	**σ_{aniso}**
N13	653.93	6410.61	N13	2635.56	6052.16	N13	871.75	595.94
N14	1621.05	5288.46	N14	6411.38	25786.03	N14	916.85	656.01
Co15	49289.45	84963.85	Cu15	16157.16	44143.15	Zn15	5.2	431.41
N16	6136.67	43276.78	N16	3203.10	17623.09	N16	273.41	716.23
N17	14002.19	27833.11	N17	8941.76	21869.78	N17	877.54	1156.93
N1	6235.13	21991.86	N1	63293.00	94223.48	N1	1551.16	1716.94

In Table 2, NMR data reported notable amounts for NO, which was adsorbed on the X–B_4N_{10}_NC as the selective sensor for detecting gas molecules in polluted air. An increase in the chemical shift anisotropy for N (1) and O (2) atoms of NO adsorption on the X–B4N10_NC was observed. The observed weak signal intensity near the parallel edge of the nanocage pattern may be due to the boron binding-induced non-spherical distribution of these complexes.

It is remarkable that doping Co, Cu, and Zn on B_4N_{10}_NC might promote the stability of nanocage, which will result in the enhanced magnetic alignment of complexes. Interestingly, the reported results show that Co, Cu, and Zn elements can be optimized to achieve optimal alignment of nanocage in the presence of an applied magnetic field.

The NO adsorption can introduce spin polarization on the X–B_4N_{10}_NC, which indicates that these surfaces might be used as magnetic scavenging surfaces for gas detection. Isotropic and anisotropic shieldings fluctuate with the occupancy in the electron accepting from gas molecules trapped in the atom-doped on the boron nitride nanocage.

Figures 4 (a–c) exhibited the same tendency of the shielding for boron and nitrogen atoms; however, a considerable deviation exists from doping atoms of Co (15), Cu (15), and Zn(15) through interaction with N (1) and O (2) of NO during adsorbing on the B_5N_{10}_NC.

In Figures 4 (a–c), NO in the complexes of NO@Co–B_4N_{10}_NC (Figure 4a), NO@Cu–B_4N_{10}_NC (Figure 4b), and NO@Zn–B_4N_{10}_NC (Figure 4c) denote the fluctuation in the chemical shielding during the trapping process.

Figures 4 (a–c) show the gap in chemical shielding between cobalt, copper, and zinc doping of X–B_4N_{10}_NC nanocage and NO. The yield of electron-accepting for doping atoms on the X–B_4N_{10}_NC through NO adsorption can be ordered as: Co> Cu >Zn > that approves the possibility of the covalent bond between cobalt, copper, zinc, and nitric oxide.

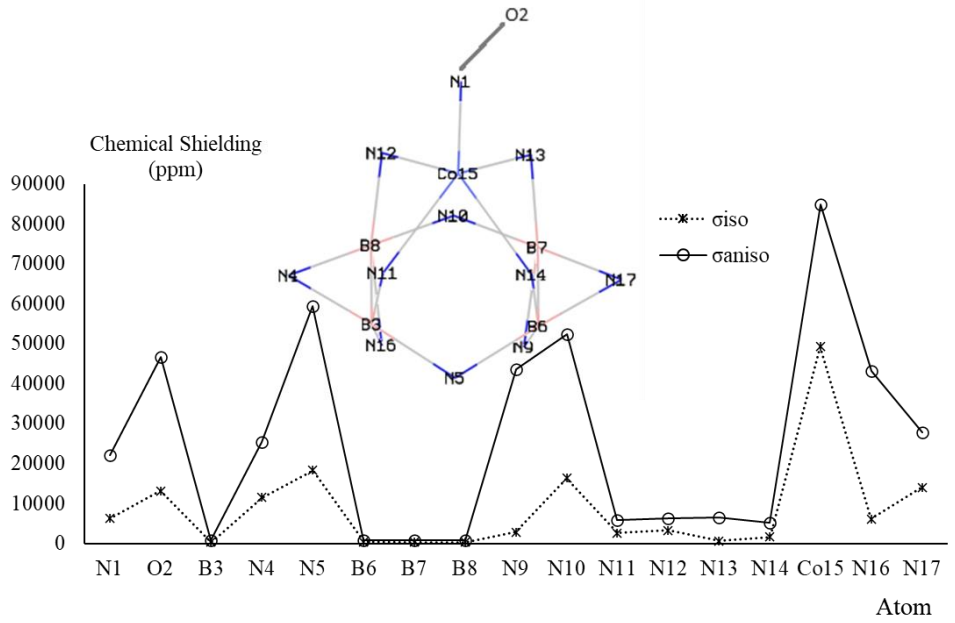

(a)

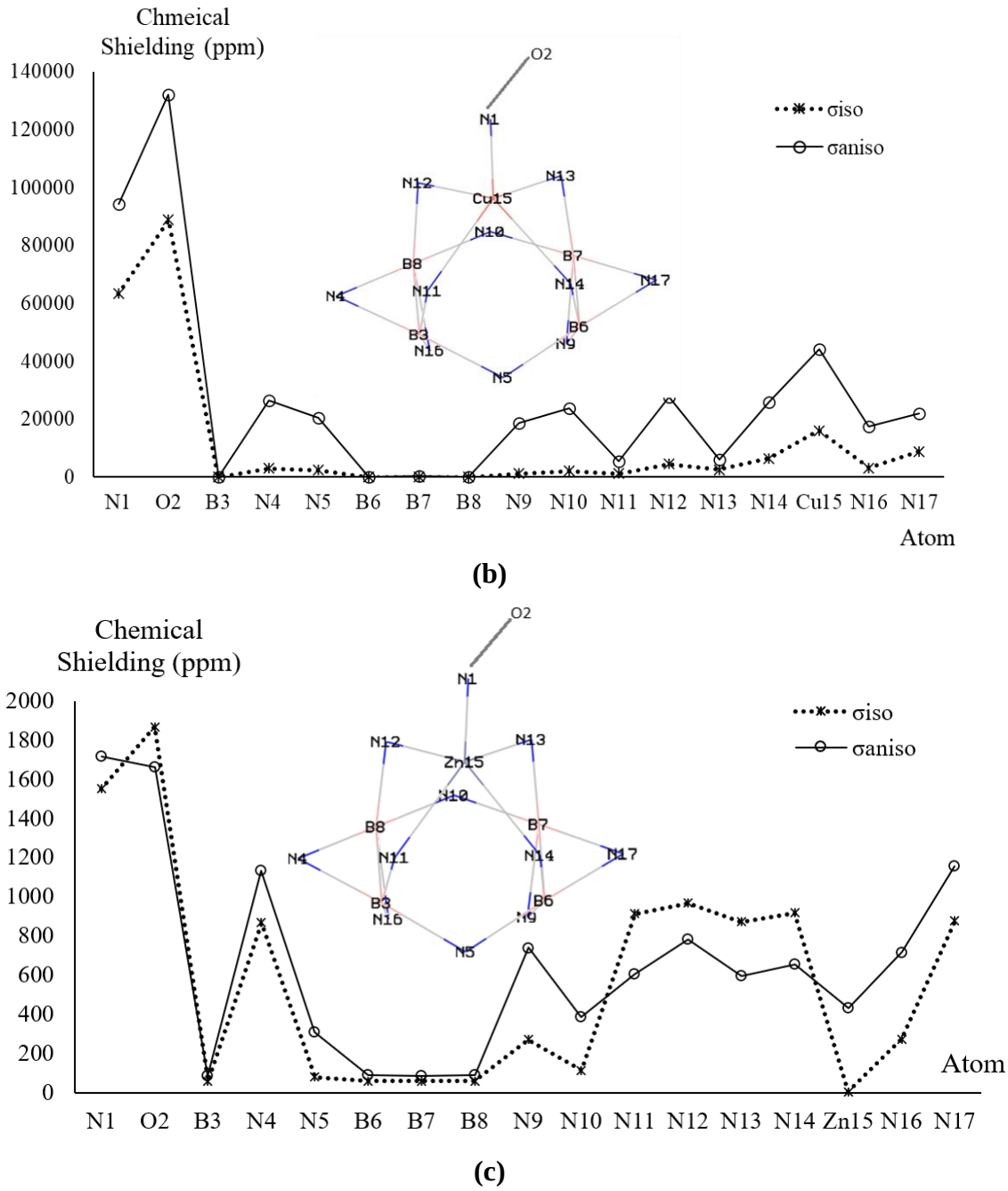

Figure 4. The NMR spectra for **(a)** NO@Co–B_4N_{10}_NC; **(b)** NO@Cu–B_4N_{10}_NC; **(c)** NO@Zn–B_4N_{10}_NC complexes using CAM–B3LYP–D3/6-311+G (d,p), LANL2DZ methods.

In the NMR spectroscopy, it has been observed the remarkable peaks around the interaction of NO molecules through adsorbing on the X–B_4N_{10}_NC during toxic gas detection and its scavenging from the polluted air; however, there are some fluctuations in the chemical shielding behaviors of isotropic and anisotropy attributes.

Therefore, the authors believe the extracted results would be useful in designing X–B4N10_NC complexes based on doped nanomaterials for increasing the NO adsorption and the structural studies using solid-state and solution NMR techniques.

3.4. IR spectroscopy and thermodynamic factors.

The IR calculations have been accomplished for the NO adsorption by X–B_4N_{10}_NC during toxic gas sensing in the polluted air. Therefore, it has been simulated the several clusters

containing NO@Co–B_4N_{10}_NC (Figure 5a), NO@Cu–B_4N_{10}_NC (Figure 5b) and NO@Zn–B_4N_{10}_NC (Figure 5c) using CAM–B3LYP–D3/6-311+G (d,p), LANL2DZ methods.

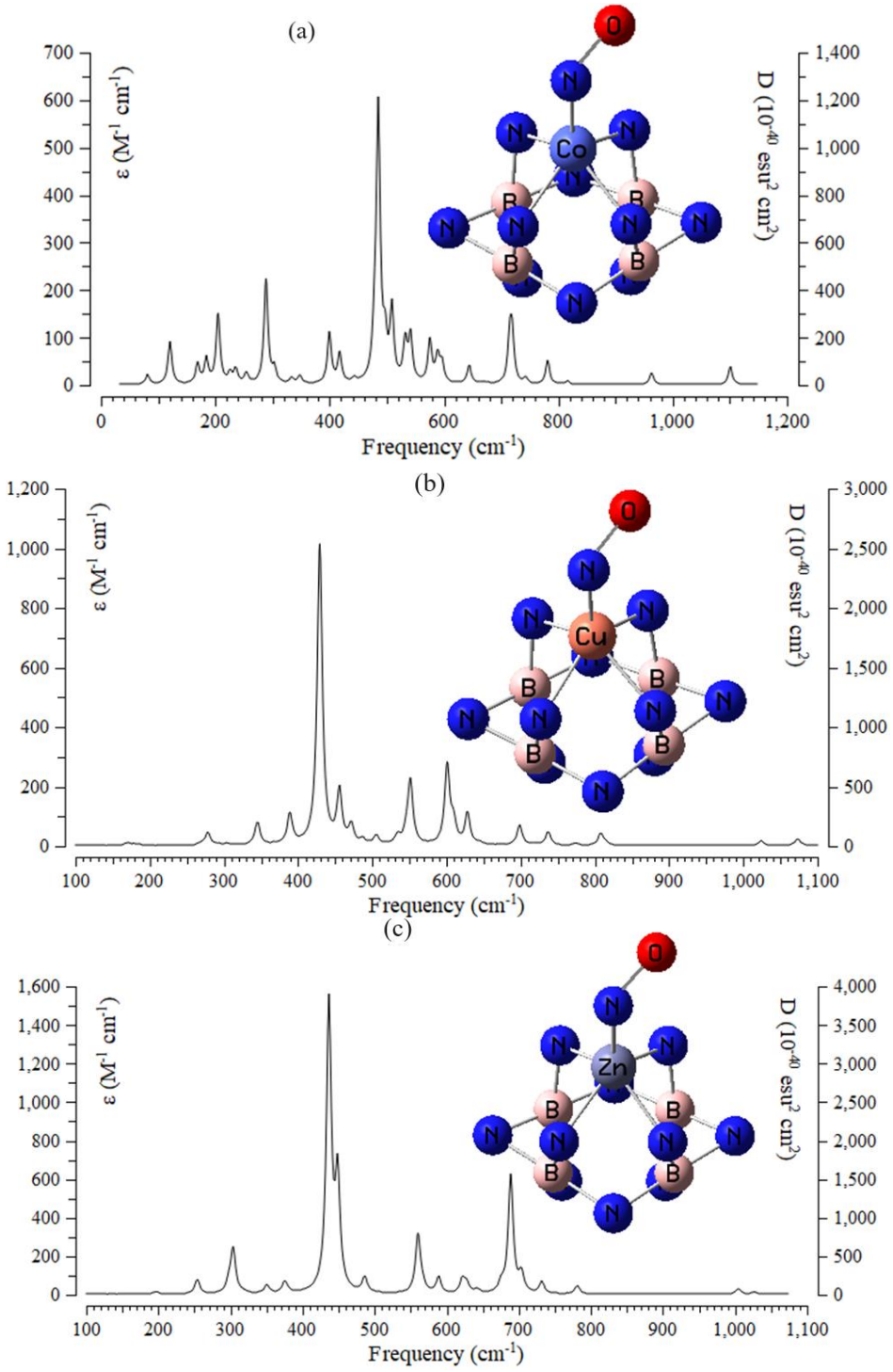

Figure 5. The Frequency (cm^{-1}) changes through the IR spectra for **(a)** NO@Co–B_4N_{10}_NC; **(b)** NO@Cu–B_4N_{10}_NC; **(c)** NO@Zn–B_4N_{10}_NC complexes using CAM–B3LYP–D3/6-311+G (d,p), LANL2DZ methods.

The graph of Figure 5a shows the frequency fluctuation between 100–1200 cm^{-1} for NO@ Co–B_4N_{10}_NC with two sharp peaks around 485.02 and 508.81cm^{-1}. Moreover, it has been observed that the frequency is between 200–1100 for NO@ Cu–B4N10_NC, with one sharp peak at around 429.12 cm-1 (Figure 5b). Besides, Figure 5c has exhibited the frequency between 200–1100 for NO @ Zn–B_4N_{10}_NC with two sharp peaks around 448.61 and 688.63 cm^{-1}.

The IR spectra of NO adsorption on the X–B_4N_{10}_NC have demonstrated that the structure of the dominant complex correlates with the electron potency of X (X= Co, Cu, Zn) doping on the B_5N_{10}_NC. As it has been seen, the doped nanocages of Co–B_4N_{10}_NC, Cu–B_4N_{10}_NC, and Zn–B_4N_{10}_NC have the most fluctuations and the highest tendencies for NO adsorption around 450 cm^{-1}. Therefore, it can be found that the IR spectroscopy for adsorbed NO on the X–B_4N_{10}_NC is now well-placed to address specific questions on the individual effect of charge carriers (gas molecule-nanocage), as well as doping atoms of the overall structure (Figure 5a–c).

Table 3, through the thermodynamic specifications, concluded that due to NO adsorption, the X–B4N10_NC complexes might be more efficient sensors for detecting and removing the noxious gas molecules from the polluted air.

Table3. The thermodynamic characters for NO@Co–B_4N_{10}_NC, NO@Cu–B_4N_{10}_NC, and NO@Zn–B_4N_{10}_NC complexes using CAM–B3LYP–D3/6–311+G (d,p), LANL2DZ methods.

Compound	$\Delta E^o \times 10^{-3}$ (kcal/mol)	$\Delta H^o \times 10^{-3}$ (kcal/mol)	$\Delta G^o \times 10^{-3}$ (kcal/mol)	S^o (cal/K.mol)	Dipole moment (Debye)
NO@Co–B_4N_{10}_NC	-577.471	-577.471	-577.503	109.405	0.5716
NO@Cu–B_4N_{10}_NC	-609.782	-609.781	-609.813	106.275	0.4199
NO@Zn–B_4N_{10}_NC	-527.877	-527.876	-527.907	103.769	0.5630

Thermodynamic parameters of NO adsorption on the X–B_4N_{10}_NC have been determined using the DFT theoretical technique. It has been shown that for a given number of nitrogen donor sites in NO, the stability of complexes owing to doping atoms of Co, Cu, Zn can be considered as: NO@Cu–B_4N_{10}_NC>>NO@Co–B_4N_{10}_NC>NO@Zn–B_4N_{10}_NC (Table 3).

The thermodynamic data in Figure 6 could detect the maximum efficiency of Co, Cu, and Zn atoms doping of B_5N_{10}_NC for NO adsorption through $\Delta G^o_{ads.}$ which depends on the covalent bond between NO and X–B_4N_{10}_NC as a potent sensor for air pollution removal.

The adsorption process of NO gas molecules on the X–B_4N_{10}_NC is affirmed by the ΔG^o_{ads} quantities:

$$\Delta G^o_{ads.} = \Delta G^o_{NO@X\text{-}B4N10\_NC} - \left(\Delta G^o_{NO} + \Delta G^o_{X\text{-}B4N10\_NC}\right); \text{X= Co, Cu, Zn} \quad (11)$$

Table 3 has shown the key role of doping of Co, Cu, Zn during the interaction between the adsorbates of NO as the electron donor and the adsorbent of Co–B_4N_{10}_NC, Cu–B_4N_{10}_NC, and Zn–B_4N_{10}_NC as electron acceptors. Therefore, the selectivity of atom-doped on boron nitride nanocage (gas sensor) for NO adsorption can result in Cu>>Co>Zn (Table 3).

4. Conclusions

This research has investigated the doping of several transition metals (Co, Cu, Zn) on the boron nitride nanocage (B_4N_{10}_NC) to enhance the toxic gas sensing of these nanomaterials to remove air pollution. Therefore, NO removal by the X–B_4N_{10}_NC has been experimented with based on the electrostatic interactions between the gas molecules and X–B_4N_{10}_NC.

The electromagnetic and thermodynamic properties of X–B_4N_{10}_NC complexes were computed using the DFT method. The results have illustrated that the chosen adsorbed NO on the X–B_4N_{10}_NC is rather stable, with the most stable adsorption site being in the center of the X–B_4N_{10}_NC system. The selectivity of atom-doped on boron nitride nanocage (gas sensor) for NO adsorption can result in NO@Cu–B_4N_{10}_NC>>NO@Co–B_4N_{10}_NC> NO@Zn–B_4N_{10}_NC, respectively.

This work proposes that the transition metals as ferromagnetic semiconductors can be examined through doping of the nanomaterials for enhancing the adsorption potential towards designing the pollution removal sensors.

Funding

This research received no external funding.

Acknowledgments

The author is grateful to Kastamonu University for successfully completing this paper and its research.

Conflict of Interest

The author declares no conflict of interest.

References

1. Gonzalez-Ortiz, D.; Salameh, C.; Bechelany, M.; Miele, P. Nanostructured boron nitride-based materials: synthesis and applications. *Mater. Today Adv.* **2020**, *8*, 100107, https://doi.org/10.1016/j.mtadv.2020.100107.
2. Mishra, N.S.; Saravanan, P. A review on the synergistic features of hexagonal boron nitride (white graphene) as adsorbent-photo active nanomaterial. *ChemistrySelect* **2018**, *3*, 8023-8034, https://doi.org/10.1002/slct.201801524.
3. Weng, Q.H.; Wang, X.B.; Wang, X.; Bando, Y.; Golberg, D. Functionalized hexagonal boron nitride nanomaterials: emerging properties and applications. *Chem. Soc. Rev.* **2016**, *45*, 3989-4012, https://doi.org/10.1039/C5CS00869G.
4. Muñoz, A.D.O.; Escobedo-Morales, A.; Skakerzadeh, E.; Anota, E.C. Effect of homonuclear boron bonds in the adsorption of DNA nucleobases on boron nitride nanosheets. *J. Mol. Liq.* **2021**, *322*, 114951, https://doi.org/10.1016/j.molliq.2020.114951.
5. Shtansky, D.V.; Matveev, A.T.; Permyakova, E.S.; Leybo, D.V.; Konopatsky, A.S.; Sorokin, P.B. Recent Progress in Fabrication and Application of BN Nanostructures and BN-Based Nanohybrids. *Nanomaterials* **2022**, *12*, 2810, https://doi.org/10.3390/nano12162810.
6. Yang, Y.; Peng, Y.; Saleem, M.F.; Chen, Z.; Sun, W. Hexagonal Boron Nitride on III–V Compounds: A Review of the Synthesis and Applications. *Materials* **2022**, *15*, 4396, https://doi.org/10.3390/ma15134396.
7. Davies, A.; Albar, J.D.; Summerfield, A.; Thomas, J.C.; Cheng, T.S.; Korolkov, V.V.; Stapleton, E.; Wrigley, J.; Goodey, N.L.; Mellor, C.J.; et al. Lattice-Matched Epitaxial Graphene Grown on Boron Nitride. *Nano Lett.* **2018**, *18*, 498–504, https://doi.org/10.1021/acs.nanolett.7b04453.
8. Bangari, R.S.; Yadav, V.K.; Singh, J.K.; Sinha, N. Fe3O4-functionalized boron nitride nanosheets as novel adsorbents for removal of arsenic(III) from contaminated water. *ACS Omega* **2020**, *5*, 10301-10314, https://doi.org/10.1021/acsomega.9b04295.
9. Chao, Y.H.; Zhang, J.; Li, H.P.; Wu, P.W.; Li, X.W.; Chang, H.H.; He, J.; Wu, H.F.; Li, H.M.; Zhu, W.S. Synthesis of boron nitride nanosheets with N-defects for efficient tetracycline antibiotics adsorptive removal. *Chem. Eng. J.* **2020**, *387*, 124138, https://doi.org/10.1016/j.cej.2020.124138.
10. Mollaamin, F.; Monajjemi,M. Trapping of toxic heavy metals from water by GN–nanocage: Application of nanomaterials for contaminant removal technique. *J. Mol. Struct.* **2024**, *1300*, 137214. https://doi.org/10.1016/j.molstruc.2023.137214.
11. Mollaamin, F.; Monajjemi, M. Transition metal (X = Mn, Fe, Co, Ni, Cu, Zn)-doped graphene as gas sensor for CO_2 and NO_2 detection: a molecular modeling framework by DFT perspective. *J Mol Model* **2023**, *29*, 119. https://doi.org/10.1007/s00894-023-05526-3.
12. Guo, Y.; Wang, R.X.; Wang, P.F.; Rao, L.; Wang, C. Developing a novel layered boron nitride-carbon nitride composite with high efficiency and selectivity to remove protonated dyes from water. *ACS Sustain. Chem.* **2019**, *7*, 5727-5741, https://doi.org/10.1021/acssuschemeng.8b05150.

13. Mollaamin, F. Competitive Intracellular Hydrogen-Nanocarrier Among Aluminum, Carbon, or Silicon Implantation: a Novel Technology of Eco-Friendly Energy Storage using Research Density Functional Theory. *Russ. J. Phys. Chem. B* **2024**, *18*, 805–820. https://doi.org/10.1134/S1990793124700131.
14. Mollaamin, F.; Shahriari, S.; Monajjemi, M. et al. Nanocluster of Aluminum Lattice via Organic Inhibitors Coating: A Study of Freundlich Adsorption. *J Clust Sci* **2023**, *34*, 1547–1562. https://doi.org/10.1007/s10876-022-02335-1.
15. Mollaamin, F.; Monajjemi, M. Tailoring and functionalizing the graphitic-like GaN and GaP nanostructures as selective sensors for NO, NO_2, and NH_3 adsorbing: a DFT study. *J Mol Model* **2023**, *29*, 170. https://doi.org/10.1007/s00894-023-05567-8.
16. Mollaamin, F.; Monajjemi, M. Adsorption ability of Ga_5N_{10} nanomaterial for removing metal ions contamination from drinking water by DFT. *Int. J. Quantum Chem.* **2024**, *124*, e27348, https://doi.org/10.1002/qua.27348.
17. Mollaamin, F.; Monajjemi, M. Metal-Doped Nitride-Based Nanostructures for Saving Sustainable and Clean Energy in Batteries. *Energy Storage* **2025**, *7*, e70122. https://doi.org/10.1002/est2.70122.
18. Hohenberg, P.; Kohn, W. Inhomogeneous Electron Gas. *Phys. Rev. B* **1964**, *136*, B864-B871, https://doi.org/10.1103/PhysRev.136.B864.
19. Kohn, W.; Sham, L. J. Self-Consistent Equations Including Exchange and Correlation Effects. *Phys. Rev.* **1965**, *140*, A1133- A1138, https://doi.org/10.1103/PhysRev.140.A1133.
20. Becke, A.D. Density-functional thermochemistry. III. The role of exact exchange. *J Chem Phys* **1993**, *98*, 5648–5652, https://doi.org/10.1063/1.464913.
21. Lee, C.; Yang, W.; Parr, R.G. Development of the Colle–Salvetti correlation-energy formula into a functional of the electron density. *Phys Rev B* **1988**, *37*, 785–789, https://doi.org/10.1103/PhysRevB.37.785.
22. Mollaamin, F.; Monajjemi, M. Determination of GaN nanosensor for scavenging of toxic heavy metal ions (Mn^{2+}, Zn^{2+}, Ag^{+}, Au^{3+}, Al^{3+}, Sn^{2+}) from water: Application of green sustainable materials by molecular modeling approach. *Comput. Theor. Chem*. **2024**, *1237*, 114646. https://doi.org/10.1016/j.comptc.2024.114646.
23. Mollaamin, F.; Monajjemi, M. The influence of Sc, V, Cr, Co, Cu, Zn as ferromagnetic semiconductors implanted on B_5N_{10}-nanocarrier for enhancing of NO sensing: An environmental eco-friendly investigation. *Comput. Theor. Chem*. **2024**, *1237*, 114666. https://doi.org/10.1016/j.comptc.2024.114666.
24. Bakhshi, K.; Mollaamin, F.; Monajjemi, M. Exchange and Correlation Effect of Hydrogen Chemisorption on Nano V(100) Surface: A DFT Study by Generalized Gradient Approximation (GGA). *J. Comput. Theor. Nanosci*. **2011**, *8*, 763–768. https://doi.org/10.1166/jctn.2011.1750.
25. Mollaamin, F.; Monajjemi, M. In Silico-DFT Investigation of Nanocluster Alloys of Al-(Mg, Ge, Sn) Coated by Nitrogen Heterocyclic Carbenes as Corrosion Inhibitors. *J Clust Sci* **2023**, *34*, 2901–2918. https://doi.org/10.1007/s10876-023-02436-5.
26. Mollaamin, F.; and Monajjemi, M. Molecular modelling framework of metal-organic clusters for conserving surfaces: Langmuir sorption through the TD-DFT/ONIOM approach. *Molecular Simulation* **2023**, *49*, 365–376, https://doi.org/10.1080/08927022.2022.2159996.
27. Mollaamin, F.; Monajjemi, M. Application of Smart Condensed H-Adsorption Nanocomposites in Batteries: Energy Storage Systems and DFT Computations. *Computation* **2024**, *12*, 234. https://doi.org/10.3390/computation12120234.
28. Frisch, M.J.; Trucks, G.W.; Schlegel, H.B.; Scuseria, G.E., Robb, M.A.; Cheeseman, J.R.; Scalmani, G.; Barone, V.; Petersson, G.A.; Nakatsuji, H.; Li, X.; Caricato, M.; Marenich, A.V.; Bloino, J.; Janesko, B.G.; Gomperts, R.; Mennucci, B.; Hratchian, H.P.; Ortiz, J.V.; Izmaylov, A.F.; Sonnenberg, J.L.; Williams-Young, D.; Ding, F.; Lipparini, F.; Egidi, F.; Goings, J.; Peng, B.; Petrone, A.; Henderson, T.; Ranasinghe, D.; Zakrzewski, V.G.; Gao, J.; Rega, N.; Zheng, G.; Liang, W.; Hada, M.; Ehara, M.; Toyota, K.; Fukuda, R.; Hasegawa, J.; Ishida, M.; Nakajima, T.; Honda, Y.; Kitao, O.; Nakai, H.; Vreven, T.; Throssell, K.; Montgomery Jr.; J.A.; Peralta, J.E.; Ogliaro, F.; Bearpark, M.J.; Heyd, J.J.; Brothers, E.N.; Kudin, K.N.; Staroverov, V.N.; Keith, T.A.; Kobayashi, R.; Normand, J.; Raghavachari, K.; Rendell, A.P.; Burant, J.C.; Iyengar, S.S.; Tomasi, J.; Cossi, M.; Millam, J.M.; Klene, M.; Adamo, C.; Cammi, R.; Ochterski, J.W.; Martin, R.L.; Morokuma, K.; Farkas, O.; Foresman, J.B.; Fox, D.J. Gaussian, Inc., Wallingford CT GaussView 5.0. Wallingford, E.U.A., **2016**.
29. GaussView, Version 6.06.16, Dennington, Roy; Keith, Todd A.; Millam, John M. Semichem Inc., Shawnee Mission, KS, **2016**.

30. Mollaamin, F.; Monajjemi, M. Doping of Graphene Nanostructure with Iron, Nickel and Zinc as Selective Detector for the Toxic Gas Removal: A Density Functional Theory Study. C–Journal of Carbon Research 2023, 9, 20. https://doi.org/10.3390/c9010020.
31. Zadeh, M.A.A.; Lari, H.; Kharghanian, L. et al. Density Functional Theory Study and Anti-Cancer Properties of Shyshaq Plant: In View Point of Nano Biotechnology. *J. Comput. Theor. Nanosci*. **2015**, *12*, 4358. https://doi.org/10.1166/jctn.2015.4366.
32. Mollaamin, F.; Monajjemi, M. Nanomaterials for Sustainable Energy in Hydrogen-Fuel Cell: Functionalization and Characterization of Carbon Nano-Semiconductors with Silicon, Germanium, Tin or Lead through Density Functional Theory Study. *Russ. J. Phys. Chem. B* **2024**, *18*, 607–623. https://doi.org/10.1134/S1990793124020271.
33. Hugh D, Y.; Roger A, F.; A Lewis, F. Sears and Zemansky's university physics: with modern physics. UNIVERSITY PHYSICS, 13rd Edition; Addison-Wesley: **2012**.
34. Sohail, U.; Ullah, F.; Binti Zainal Arfan, N.H.; Abdul Hamid, M.H.S.; Mahmood, T.; Sheikh, N.S.; Ayub, K. Transition Metal Sensing with Nitrogenated Holey Graphene: A First-Principles Investigation. *Molecules* **2023**, *28*, 4060, https://doi.org/10.3390/molecules28104060.